ACS APPLIED MATERIALS & INTERFACES

Research Article

Cite This: ACS Appl. Mater. Interfaces 2018, 10, 42915−42924

www.acsami.org

Bright Yellow Fluorescent Carbon Dots as a Multifunctional Sensing Platform for the Label-Free Detection of Fluoroquinolones and Histidine

Wenjing Lu,[†,‡,∥] Yuan Jiao,[†] Yifang Gao,[†] Jie Qiao,[§,‡] Maedeh Mozneb,[‡] Shaomin Shuang,[†] Chuan Dong,*[,†] and Chen-zhong Li*[,‡]

[†]Institute of Environmental Science, and School of Chemistry and Chemical Engineering, Shanxi University, Taiyuan 030006, China

[‡]Nanobioengineering/Bioelectronics Laboratory, and Department of Biomedical Engineering, Florida International University, Miami 33174, United States

[§]School of Basic Medical Sciences, Shanxi Medical University, Taiyuan 030001, China

Supporting Information

ABSTRACT: Owing to their diverse properties, fluorescent carbon dots (CDs) have attracted more attention and present enormous potential in development of sensors, bioimaging, drug delivery, microfluidics, photodynamic therapy, light emitting diode, and so forth. Herein, a multifunctional sensing platform based on bright yellow fluorescent CDs (Y-CDs) was designed for the label-free detection of fluoroquinolones (FQs) and histidine (His). The Y-CDs with superior optical and biological merits including high chemical stability, good biocompatibility, and low cytotoxicity were simply synthesized via one-step hydrothermal treatment of *o*-phenylenediamine (*o*-PD) and 4-aminobutyric acid (GABA). The Y-CDs can be utilized to directly monitor the amount of FQs based on fluorescence static quenching owing to the specific interaction between FQs and Y-CDs. Then, the fluorescence of this system can be effectively recovered upon addition of His. The multifunctional sensing platform exhibited high sensitivity and selectivity toward three kinds of FQs and His with low detection limits of 17−67 and 35 nM, respectively. Benefiting from these outstanding characters, the Y-CDs were successfully employed for trace detection of FQs in real samples such as antibiotic tablets and milk products. Furthermore, the probe was also extended to cellular imaging. All of the above prove that this multifunctional sensing platform presents great prospect in multiple applications such as biosensing, biomedicine, disease diagnosis, and environmental monitoring.

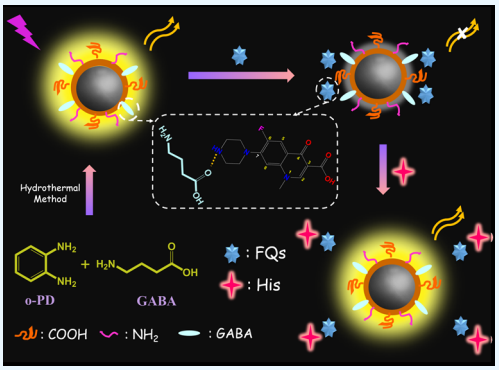

KEYWORDS: *carbon Dots, fluoroquinolones, histidine, label-free detection, multi-functional sensor, cellular imaging*

1. INTRODUCTION

Fluoroquinolones (FQs) are the third generation synthetic quinolone antibiotic drugs and have been utilized for over 50 years since the development of the first fluoroquinolone norfloxacin (NOR) was synthesized in the 1970s.[1−3] As a useful chemotherapeutic antibacterial, FQs have been generally used in veterinary and human medicine in the treatment and prevention of various pathogenic bacterial infections, for instance lower respiratory tract infections, urinary tract infections, and pulmonary and intraabdominal infections.[4−7] They demonstrated broad-spectrum antibacterial activity against both Gram-positive and Gram-negative bacteria by the inhibition of DNA gyrase, which caused an irreversible damage to bacterial DNA.[8−10] In recent years, with the widespread use of these antibacterial agents, the excess FQs will remain in surface water, soil, and animal foods such as fish, shrimp, and milk products. They reveal a potential public health hazard even in low concentration, because of their toxicity and allergy reactions, which can lead to liver damage, thrombus, central nervous system (CNS) injury, and drug resistance of microbial strains.[11,12] Therefore, the European Union (EU) has limited maximum residue of FQs in various animal-produced foods.[13] In addition, China's Ministry of Agriculture (CMA) has also forbidden the use of some FQs in animal feed.[14] Consequently, effective monitoring of FQ residues has become a crucial issue.

To date, there are several analytical techniques that have been developed to monitor FQ residues in real agri-food samples, pharmaceutical formulations, and biological fluids, which are divided into two categories: instrumental analytical methods and immunoassays. The instrumental analytical methods include high-performance liquid chromatography

Received: September 25, 2018
Accepted: November 9, 2018
Published: November 9, 2018

DOI: 10.1021/acsami.8b16710
ACS Appl. Mater. Interfaces 2018, 10, 42915−42924

(HPLC),[15] liquid chromatography−electrospray ionization−tandem mass spectrometry (LC−ESI−MS/MS),[16] capillary electrophoresis (CE),[17] surface-enhanced Raman spectroscopy,[18] and electrochemistry.[19] Immunoassays are used usually based on antigen−antibody recognition including enzyme-linked immunosorbent assay[20] and immunochromatographic assay.[21] These methods show high-throughput screening, great sensitivity, and accuracy. However, most of them usually involve some unavoidable drawbacks such as requiring expensive and sophisticated instruments, undergoing bad reproducibility, and time-consuming sample pretreatment, which limit their use in real-time field analysis of the samples. Recently, to solve these problems, some scientists have developed biosensors based on novel nanomaterials to detect FQs for clinical diagnosis. For example, Tang et al.[22] synthesized a core−shell upconversion particle-based probe UCPs@Fe_3O_4@MIP combined with magnetism and molecular recognition. They used this novel fluorescent probe to detect multiple quinolones in fish samples. In addition, Mao et al.[23] set up the Ag nanocluster−Cu^{2+} sensing system with the fluorescence turn-on mode for the trace detection of quinolones. However, a lot of these methods usually need to bond with metal ions (e.g., Eu^{3+} and Cu^{2+}) or molecularly imprinted polymer,[24,25] which causes the preparation process complex. Hence, it is of considerable importance and very desirable to develop a convenient, good sensitivity, outstanding selectivity, and high-throughput method to trace the level of FQs in the food and environmental samples.

Histidine (His) is an essential amino acid and is of great importance in the function of many proteins for the growth and repair of tissues and organs. It not only acts as a crucial neurotransmitter or neuromodulator in human and other mammalian CNSs but also controls the transmission of metal elements in biological systems.[26,27] The unbalance of histidine expression is usually associated with numerous diseases such as rheumatoid arthritis, liver failure, pulmonary disease, AIDS, Alzheimer's disease, and cancer.[28−30] Owing to its vital biological functions, multiple approaches have been built to detect histidine. In addition to the traditional analytical techniques such as CE,[31] HPLC,[32] spectrophotometry,[33] and electrochemistry,[34] fluorescent biosensors have been extensively employed to monitor histidine because of their simple operation, excellent selectivity, and sensitivity. However, it is worthy of attention that the detection mechanisms of many reported His sensors are based on metal complexes. Especially, the divalent metal ions are widely used (including Cu^{2+}, Co^{2+}, and Ni^{2+}) and selected by their good histidine affinity. For instance, Cu^{2+}-mediated DNA-templated silver nanoclusters,[35] G-quadruplex-Cu(II) metalloenzyme,[36] naphthalimide@Cu^{2+}-based fluorescent sensors,[37] and Co^{2+}-adsorbed Mn:ZnS quantum dot probes[38] have been exploited as a turn-on fluorescent or phosphorescence sensor for tracing of His. Even so, they still have some drawbacks such as complex synthesis procedures, high toxicity, and the fact that they can be used only in organic solution. As a result, it is imperative to design a simple and high-efficiency analytical technique for the assessment of histidine in aqueous solution especially in biological systems, which has important research significance to understand the pathogenesis for clinical therapy.[39]

As the newest generation of carbon nanomaterials in the past decade, carbon dots (CDs) have presented tremendous potential in various applications such as sensors, bioimaging, drug delivery, microfluidics, photocatalysts, light emitting diode (LED), and so forth[40−42] owing to the characteristics of a simple preparation process and excellent electrical or optical properties. In many applications, CDs are widely used as chemical sensors and biological sensors.[43,44] The objects of detection are very extensive and cover chemical, environmental, and biological field, for instance pH, heavy metals, amino acids, bioenzymes, free radicals, and so on.[45−47] Meanwhile, CDs have become promising candidates as a new generation of fluorescent reagents for bioimaging, including in multiple living cells, even in vivo tissues of mice and zebrafish.[48] All these stem from the low toxicity and good biocompatibility of CDs. With the researche studies of the CDs gradually deepening, the properties of CDs can be attributed to several factors including the size distribution, surface states, and charge transfer.[49−51] However, it is still hard to establish sufficient theoretical conclusions to explain the properties of CDs, and scientists design different methods to synthesize CDs with different properties for diverse applications. In order to achieve the specific requirements in practical applications, the purposeful surface functionalization on the surface of CDs has gained considerable attention.[52−54] Nevertheless, this will present many problems, for instance, the time-consuming preparation processes due to the complicated chemical modification steps, the instability caused by environmental factors (such as solvents used and pH etc.), and the affected luminescent properties.[55,56] Besides, most of the currently reported CDs' emission is concentrated in blue to green light regions, which restrict their further applications in biomedical and optical optoelectronic devices. It is of profound significance to achieve long wavelength emissive (such as yellow or red light) CDs.[57] Thus, it sorely needs to structure a novel, simple, and controllable method to synthesize the self-functional CDs with long emission wavelength for multi-purpose applications.

Inspired by the above circumstances, we designed a multifunctional sensing platform based on CDs for the label-free detection of FQs and histidine (His) (Scheme 1). The obtained CDs were synthesized through the one-step hydrothermal synthesis route by taking *o*-phenylenediamine (*o*-PD) and 4-aminobutyric acid (GABA) as the precursors. Owing to the effects of raw materials to the properties of CDs, the as-prepared CDs (Y-CDs) emitted bright yellow fluorescence. On account of their good tissue penetration, Y-CDs manifest more application potential than the blue or green fluorescent CDs in

Scheme 1. Schematic Illustration of the Multifunctional Sensor for the Direct Detection of FQs and His Based on the Fluorescence Y-CDs

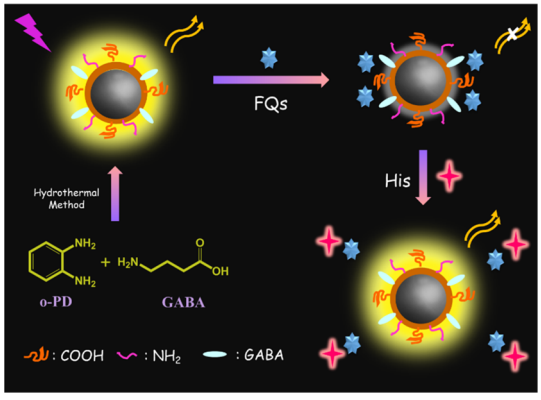

DOI: 10.1021/acsami.8b16710
ACS Appl. Mater. Interfaces 2018, 10, 42915−42924

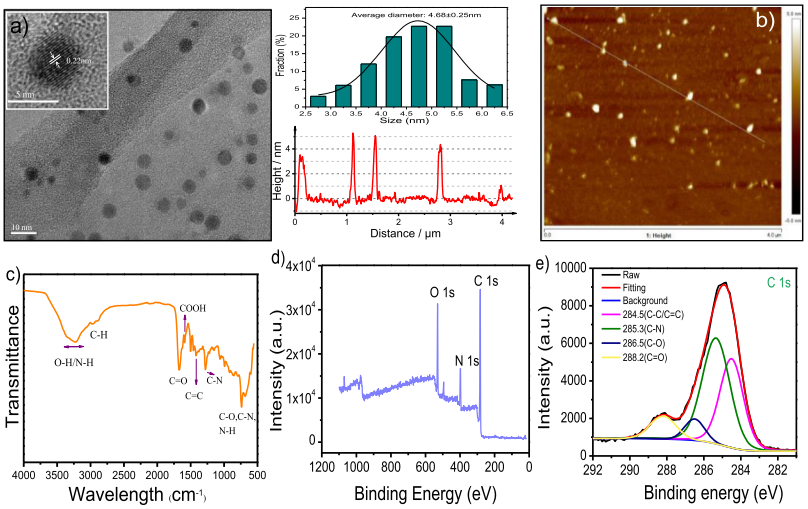

Figure 1. (a)TEM, HRTEM (inset) images, and the size distribution of the Y-CDs. (b) AFM image, (c) FTIR, (d) XPS survey, and (e) C 1s spectra of the Y-CDs.

the biomedical field. In addition, because the surface of Y-CDs retained the relevant functional structures of the precursor GABA, it could interact with FQs and disrupted the surface states of Y-CDs, and the fluorescence of Y-CDs was significantly decreased in the presence of FQs. Thus, the Y-CDs can be utilized as a label-free fluorescence probe for the trace detection of FQs without any complicated functionalization, including norfloxacin (NOR), ciprofloxacin (CIP), and ofloxacin (OFX). This probe is simple to prepare and easy to operate. Interestingly, when adding histidine to the Y-CDs−FQs system subsequently, the Y-CDs were preferably exchanged for His to form a more stable FQs−His complex. As a consequence, the fluorescence of the system was observably recovered. Therefore, the Y-CDs−FQs system can selectively sense histidine. This Y-CDs multifunctional sensing platform used a simple operation process and exhibited good selectivity and sensitivity. In addition, the present sensor has realized the detection of FQs' amount in real samples, such as antibiotic tablets and milk samples. The results manifested that the new sensing platform would be a promising tool for monitoring of antibiotic residues and the drug quality control analysis. Moreover, the Y-CDs−FQs system as a "turn-on" probe was also successfully employed in intracellular imaging for detection of His because of good biocompatibility and low toxicity.

2. EXPERIMENTAL SECTION

2.1. Materials. *o*-phenylenediamine (*o*-PD), 4-aminobutyric acid (GABA), erythromycin (ERY), and streptomycin sulfate (STR) were obtained from Acros Organics (USA). Norfloxacin (NOR), ciprofloxacin hydrochloride (CIP), ofloxacin (OFX), oxytetracycline (OTC), ampicillin sodium salt (AMP), and chloramphenicol (CHL) were obtained from Alfa Aesar (USA). Amino acids were purchased from Sigma-Aldrich Chemical Co. (USA).

2.2. Synthesis of Y-CDs. The Y-CDs were synthesized by the one-pot hydrothermal method. Typically, for the Y-CDs, *o*-PD (0.3244 g) and GABA (0.3093 g) were first completely dissolved in 20 mL of ultrapure water under ultrasonic vibration for 15 min, and the solution was transferred into a Teflon autoclave with heating at 160 °C for 8 h. Then, the autoclave was cooled down to room temperature naturally. Subsequently, the product was diluted 5 times by ultrapure water. The solution of produced Y-CDs was centrifuged at 11 000 rpm for 15 min to remove any deposits. Next, the supernatant was dialyzed through a dialysis membrane (MWCO 1/4 500−1000) for 72 h after filtering by a 0.22 μm pore diameter microporous membrane. Last, the solid-state Y-CDs were collected by freeze-drying.

2.3. Detection of FQs and His. The Y-CDs were mixed with phosphate-buffered saline (PBS) solution (10 mM, pH 7.4) and put into a solution with the final concentration of 0.2 mg mL^{-1}. For the detection of FQs, using NOR as the model, FL measurement of the Y-CDs was collected by adding different concentrations of NOR. For the titration of Y-CDs−NOR with His, different concentrations of His were added into the Y-CDs−NOR (0.2 mg·mL^{-1} and 50 μM, respectively) system and recording the fluorescence intensity was recorded. The selectivity of the sensor toward FQs and His was evaluated by adding other antibiotics, amino acids, biologically related substances, or ions instead of FQs or His in a similar way as mentioned above.

2.4. Detection of FQs in Antibiotic Tablets. The method was used to detect NOR tablets, CIP tablets, and OFX tablets. Each antibiotic tablets was ground to a fine powder after being weighed accurately and diluted with ultrapure water to an appropriate concentration. Finally, the solutions were analyzed by the Y−CDs.

2.5. Detection of FQs in Milk Samples. Cow's milk samples were purchased from local markets. The treatment method refers to the literature.[58] To precipitate proteins and extract residual drugs, 5.0 mL of the milk sample was transferred into a centrifuge tube and heated to 80 °C in a water bath for 10 min. After cooling to room temperature, 0.5 mL of acetonitrile was added slowly into the sample with vigorous mixing. Next, the pH value of the supernatant was adjusted to neutrality using NaOH. Then, the mixture was centrifuged at 10 000 rpm for 10 min and filtered by using a 0.22 μm membrane. Finally, the filtrate was collected and supplemented with three different concentrations (0.5, 5, and 10 μM) of standard FQs solutions. All of the samples were stored at 4 °C before used.

2.6. Cell Imaging. SMMC 7712 cells were incubated in the RPMI1640 medium at 37 °C for 24 h. Subsequently, the SMMC 7712 cells were incubated with the fresh 0.2 mg mL^{-1} Y-CDs for 3 h. Next, the excess medium was removed and each dish was washed three times with 1.0 mL of PBS buffer (pH 7.4). Following that, cellular fluorescence imaging was performed with an Airyscan LSM 880 laser scanning confocal microscope. Then, to verify the actual applicability of Y-CDs as a fluorescent probe for detection of NOR and His in living cells, fluorescence images of the treated cells were acquired by laser scanning confocal microscopy (LSCM). The treated cells were sequentially added with 10 μL of NOR (5.0 mM) and 2.0 μL of His (5.0 mM).

DOI: 10.1021/acsami.8b16710
ACS Appl. Mater. Interfaces 2018, 10, 42915−42924

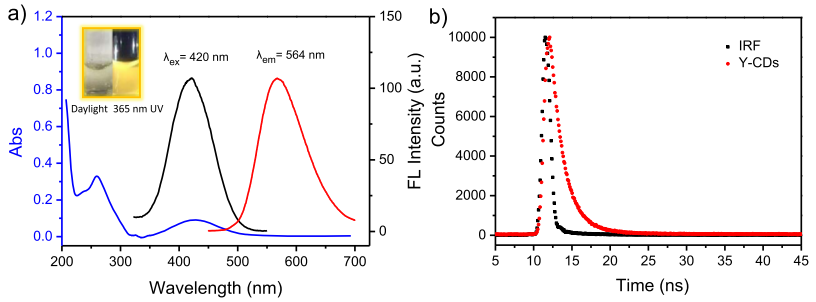

Figure 2. (a) UV−vis absorption and FL spectra of the Y-CDs. Insert: the pictures of Y-CDs under daylight (left) and 365 nm UV light (right). (b) FL decay curves of Y-CDs. The concentration of Y-CDs samples is 0.20 mg mL^{-1}.

3. RESULTS AND DISCUSSION

3.1. Characterization of Y-CDs. The yellow fluorescence carbon nanodots (Y-CDs) were prepared by the typical hydrothermal route using *o*-PD and GABA. The synthesis of Y-CDs has been recorded in detail in the previous Experimental Section. First, the morphology and structure were investigated. Transmission electron microscopy (TEM) analysis proves that the Y-CDs appear uniform and form monodisperse spheres. They have a narrow distribution in the range of 2.75−6.25 nm and the average diameter is between 4.68 ± 0.25 nm (Figure 1a). In more detail, the high-resolution TEM (HRTEM) image displays that Y-CDs present the graphite-like crystalline structure with obvious interlayer lattice fringes of 0.22 nm, which corresponds to the (100) plane of graphite carbon.[59] The atomic force microscopy (AFM) imaging in Figure 1b displays that the height of Y-CDs is found to be 4.38 nm, which is in line with the TEM results.

Then, the elemental analysis and surface composition of the Y-CDs were explored. Elemental analysis in Table S1 represents the content of the elements which constitute Y-CDs: % wt of C 60.30%, H 6.09%, N 22.94%, and O (calculated) 10.67%. The Fourier transform infrared (FTIR) spectrum (Figure 1c) shows the broad absorption band at 3100−3400 and 2890−2950 cm^{-1} which are attributed to the stretching vibration of O−H/N−H and C−H, respectively.[60] The sharp absorption peaks at 1671 and 1641 cm^{-1} corresponded to the amide carbonyl (CONH) and carboxyl (COOH) groups, respectively.[61] Moreover, the absorption peaks at 1500 and 1400 cm^{-1} are assigned to C═C and C−N from stretching vibrations,[62] respectively. In addition, Y-CDs with absorption peaks at 1000−1300 cm^{-1} are ascribed to the C−O, C−N, and N−H bonds.[63] Also, X-ray photoelectron spectra (XPS) (Figure 1d) showed that the C 1s, N 1s, and O 1s peaks of Y-CDs were observed at 285.0, 400.0, and 532.0 eV, respectively. The high-resolution C 1s XPS spectrum could be decomposed into four peaks at 284.5 eV (C−C/C═C), 285.3 eV (C−N), 286.5 eV (C−O), and 288.2 eV(C═O), respectively (Figure 1e). The N 1s spectrum was observed to be divided into three components at 398.8, 399.7, and 401.4 eV, matched with pyridine C−N═C, N−C, and graphitic N−C_3,[64] respectively (Figure S1a). The high-resolved O 1s XPS spectrum exhibited the distinctive peaks of C−OH and C═O at 531.3 and 532.4 eV,[62] respectively (Figure S1b). The XPS spectra analysis further confirmed the results of FTIR.

3.2. Optical Properties of Y-CDs. Subsequently, UV−vis absorption, fluorescence spectra, and quantum yield (QY) were utilized to examine the optical properties and photoluminescence mechanism of Y-CDs. In UV−vis absorption spectra (Figure 2a), Y-CDs exhibited two obvious absorption peaks at 260 and 427 nm. The absorption peak at 260 nm was considered as the core state accompanied by the highest energy level, which was ascribed to the $\pi-\pi^*$ transition by sp^2 domains. The wide absorption band at 427 nm could be denoted as the surface state, which consists of a set of low-energy absorption bands such as the functional groups attached to the surface of Y-CDs.[65] As shown inFigure 2a, bright yellow fluorescence was observed for the as-prepared Y-CDs upon the 365 nm UV light irradiation. In the fields of bioimaging or biomedicine, the Y-CDs with yellow fluorescence not only have good tissue penetration but also will avoid the general blue-auto fluorescence of the biological matrix. Therefore, they have favorable application potential.[57] In fluorescence spectra, the Y-CDs manifested a maximum emission wavelength centered at 564 nm when excited at 420 nm. The yellow fluorescence of Y-CDs possibly derives from the conjugated aromatic π systems and surface states of nitrogen-related speciation because the precursor *o*-PD has a benzene ring structure and GABA is rich in amino. When forming Y-CDs, the structures of two precursors and their deformations will be connected to the surface of the carbon core, which are conducive to formation of conjugated aromatic π systems and doping nitrogen into the domains, eventually forming the emission states on the surface of Y-CDs. According to the numerous research studies, the conjugated aromatic π systems result in the redshift of absorption and emission wavelength. Meanwhile, as the XPS results showed, part of N atoms will form pyridine N and graphitic N−C_3 on the surface of the Y-CDs, which can not only help Y-CDs to form more efficient conjugated aromatic π systems but also build up a number of nitrogen-related energy states and reduce the energy gap. The energy level of these surface states was under the LUMO of core states from $\pi-\pi^*$ transitions in Y-CDs, resulting in a yellow fluorescent emission.[65,66] Then, by increasing λ_{ex} from 300 to 520 nm, the Y-CDs showed an excitation-independent character with λ_{em} at 564 nm, which illustrated that a nearly uniform emission state consists in the Y-CDs surface (Figure S2). The QY of the Y-CDs was calculated to be 22.6%, by choosing rhodamine 6G in ethanol as the reference. The average fluorescence lifetime of Y-CDs is about 2.828 ns (Figure 2b).

The optical stability of Y-CDs was investigated. As shown in (Figure S3a), the Y-CDs revealed great luminescence stability under 120 min of continuous illumination by xenon arc light. Furthermore, the relative fluorescence intensity of Y-CDs decreased in a strong acidic or alkali solution but still remained steady on broad pH ranges (4−12, in PBS solution) (Figure S3b). Additionally, Figure S3c depicts that the Y-CDs possessed excellent patience even in a high ionic strength

DOI: 10.1021/acsami.8b16710
ACS Appl. Mater. Interfaces 2018, 10, 42915−42924

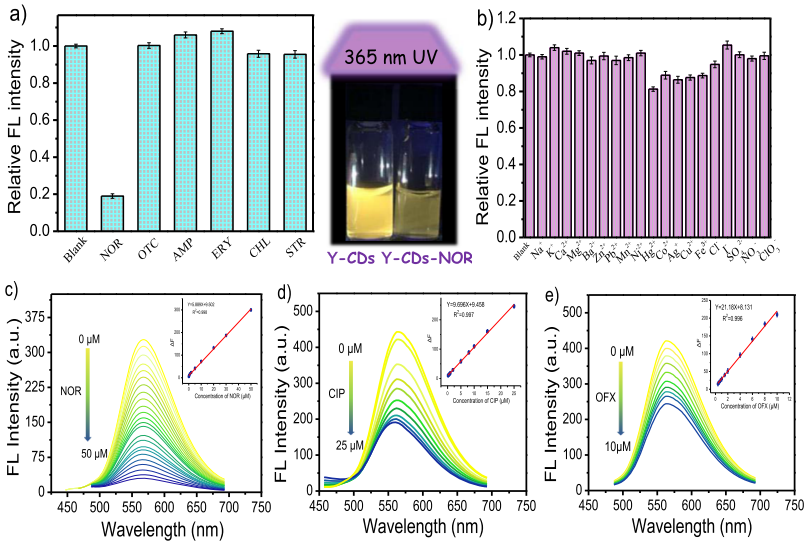

Figure 3. Relative FL intensity of Y-CDs in the presence of different (a) antibiotics and (b) ions. Insert: the photographs of fluorescent Y-CDs solution before and after adding NOR under 365 nm UV light. (c–e) Fluorescence spectra of Y-CDs upon adding different concentrations of NOR (from top to bottom, 0–50 μM), CIP (0–25 μM), and OFX (0–10 μM). Insert: the linear relationship between ΔF and the concentrations of (c) NOR, (d) CIP, and (e) OFX. The error bars represent standard deviations based on three independent measurements.

surrounding of 2 M NaCl solution. All the above evidences properties indicate that Y-CDs as a fluorescence probe have great potential for analysis of complex samples.

3.3. Label-Free FQ Sensing Based on Y-CDs. Because a large number of active structures exist on the surface of the Y-CDs, we explored the potential application in sensors. Unexpectedly, Y-CDs as a fluorescent probe can directly detect FQs. The introduction of FQs brings significant fluorescence quenching of Y-CDs. For exploration of the quenching mechanism, the fluorescence lifetime measurements were employed to distinguish the quenching type of this process. As indicated in Figure S4 and Table S2, the fluorescence emission decay curves and the lifetime data of the system before and after adding three kinds of FQs (including NOR, CIP, and OFX Figure S5) shows no significant changes. The results indicated a static quenching process occurring between Y-CDs and FQs. Meanwhile, using NOR as a model compound, we observed the UV–vis absorption spectra in the sensing system. Figure S6a displays that the peak of Y-CDs at 427 nm (originated in the surface states) undergoes a significant disappearance, and a new absorption peak arises at 451 nm after adding NOR. This phenomenon may be caused by the complexation reaction between NOR and Y-CDs to form a stable composite, which changes the surface functional groups of Y-CDs and leads to static fluorescence quenching. To verify this inference, the effect of temperature on fluorescence quenching was explored because the temperature rise may affect the stability of the complex, thereby reducing the degree of static quenching. As shown in Figure S6b, the system conforms to the static quenching equation $F_0/F = 1 + K[Q]$. When the temperature of the system rises from 25 to 37 °C, the complexation constant of the reaction decreases from 8.02×10^3 to 5.93×10^3 L·mol^{-1}. All of these prove that FQs can make the fluorescence of Y-CDs static quench. According to the literature, the position C7 side-chain substituents of the FQs can inhibit the binding of neurotransmitter GABA to the receptor, increasing the excitability of the CNS and leading to epilepsy and other neurological diseases. Notably, the FQs with nonsubstituted piperazine on the C7 position (such as NOR and CIP) exhibit the strongest inhibition of GABA.[67,68] In addition, the surface of the Y-CDs may have retained the active structure of the precursor GABA during the synthesis process. Therefore, these conditions provide the possibility for FQs to interact strongly with Y-CDs and form a Y-CD–FQ complex. To prove this, the FL and FTIR spectra of A-CDs (performed by using alanine as a precursor to replace GABA) and R-CDs (reduced Y-CDs by $NaBH_4$) were recorded. No fluorescence quenching occurred when NOR was introduced to the two kinds of CDs (Figure S7), indicating the necessity of raw material GABA. Moreover, as shown in FTIR spectra (Figure S8), the Y-CDs retained most of the GABA structures than the other two CDs. For example, the FTIR spectrum of Y-CDs exhibits the same absorption peaks with GABA at 1428 and 1122 cm^{-1} attributed to the δ_{H-C-H} and ω_{H-N-H}, respectively.[69] Hence, all evidence supports the efficacy of Y-CDs as a fluorescence sensor for label-free detection of FQs. When FQs are introduced to the Y-CD system, a strong interaction occurs between the C7 position side-chain substituents of the FQs and the active structure of GABA or other surface groups on the Y-CD surface, which generates the formation of the Y-CD–FQ complex and disrupts the surface state of Y-CDs, thus causing the quenching phenomenon of Y-CDs. Further mechanisms will be explored in future works. In addition, owing to the significance of raw materials to the properties of CDs, it is promising to prepare CDs with excellent properties by the active structure preservation (ASP) method.[54]

The selectivity of Y-CDs as a label-free probe for detection of FQs was assessed by measurement of the FL spectra of Y-CDs to other types of antibiotics, metal ions, and certain anions. As shown in Figure 3a, compared with NOR, the effect of five other types of antibiotics (ERY, STR, OTC, AMP, and CHL) on the relative FL intensity of Y-CDs is negligible. Only NOR could distinctly turn off the yellow fluorescence of the Y-CDs. When introducing various ions to Y-CDs, the relative FL intensity of Y-CDs has little significant change (Figure 3b). This implies that this label-free sensor can recognize FQs from

DOI: 10.1021/acsami.8b16710
ACS Appl. Mater. Interfaces 2018, 10, 42915–42924

other substances and displays outstanding selectivity. Also, fluorescence titrations under optimal conditions were conducted to evaluate the sensitivity of the label-free sensor for three FQs including NOR, CIP, and OFX. As shown in Figure 3c–e, with the concentration of FQs rising, it was observed that the FL intensity of Y-CDs declined gradually. ΔF ($\Delta F = F - F_0$, where F and F_0 represent the FL intensity of the Y-CDs in the absence and presence of FQs) exhibited a good linear response to the concentration of FQs (insert in Figure 3c–e). The linear range was 0.05–50 μM for NOR, 0.2–25 μM for CIP, and 0.4–10 μM for OFX. The limit of detections (LODs) of NOR, CIP, and OFX were calculated to be 17, 35, and 67 nM, respectively (based on S/N = 3, Table 1). It should be noted that NOR and CIP displayed better sensitivity and a lower LOD than OFX. This result is probably because the nonsubstituted piperazine on the C7 position of NOR and CIP reveals a stronger interaction with the groups on the Y-CD surface than methyl-substituted piperazine on the C7 position of OFX. In summary, Y-CDs' sensing capabilities have great potential to be used for detecting FQs in the complex samples with sensitivity comparable or superior to the previous works (Table S3).

Table 1. Analysis Parameter of the Sensor for Detection of FQs[a]

analytes	linear range μmol L^{-1}	R^2	LOD nmol L^{-1}
NOR	0.05–50	0.9985	17
CIP	0.2–25	0.9973	35
OFX	0.4–10	0.9961	67

[a]The detection limits were calculated by using S/N = 3.

3.4. His-Sensing Platform with the Y-CDs–FQs System in a"Turn-On" Mode. Surprisingly, we observed that the quenched fluorescence of Y-CDs–NOR can be recovered with the introduction of histidine (His). In addition, Y-CDs–CIP and Y-CDs–OFX complexes shared the similar property with Y-CDs–NOR of FL intensity recovery upon His addition (Figure S9). The results showed that the Y-CDs–FQs system has the potential to monitor levels of His in a "turn-on" mode. To explain this phenomenon, the UV–vis absorption spectra in this sensing system were recorded. Using Y-CDs–NOR solution as an example, when adding His, the band at 451 nm disappeared immediately and the previous peak of Y-CDs at 427 nm appeared again (Figure S10). These phenomena can probably be attributed to FQs expressing a stronger affinity toward His and formation of a more stable complex FQs–His. The competitive coordination of His would take FQs off the surface of Y-CDs, which causes the absorption band and surface states of Y-CDs to return to its original level. As a result, the electron transfer process of Y-CDs returns to its original path and the fluorescence of the system is dramatically restored. Besides, according to the literature,[70] NOR could induce the photooxidation decomposition of His, which indicated a special interaction between NOR and His. Therefore, we will continue to delineate the most likely mechanism in future studies. Scheme 2 described a possible sensing tactic.

We choose the Y-CD–NOR system for subsequent experiments because of the superior sensitivity of Y-CD–NOR detection of His. Then, we compared other amino acids as control samples to demonstrate the selectivity of His to the Y-CD–NOR system. Figure 4a demonstrates that only His could lead to the significant increase of fluorescence intensity, and the influence of other amino acids on the sensor was negligible. Furthermore, we carried out the fluorescence response of Y-CDs–NOR toward various potentially coexisting substances in live cells, such as Na^+, K^+, Mg^{2+}, Ca^{2+}, Zn^{2+} (2.0 mM), glucose, GSH, human serum albumin, bovine hemoglobin, urea, oxalic acid, ascorbic acid, and citric acid (1.0 mM). As displayed in Figure S11, the FL intensity of Y-CDs–NOR shows no significant change (less than 10%) by the introduction of common biologically related substances with higher concentration. Moreover, the sensing platform is largely unaffected by the pH of the surrounding environment (Figure S12). All these reveal that the sensing platform displays superior selectivity and meets the requirements for bioimaging applications. Figure 4b shows the change of the FL intensity of Y-CDs–NOR with the increase of His. Introducing His slowly brought a remarkable fluorescence recovery of about 95% of the original fluorescence intensity. The detection limit is estimated to be 35 nM with a relative standard deviation (RSD) of 3.75% and good linear range of 0.05–10 μM (Figure 4b insert). The Y-CD–NOR system displayed superior sensitivity when compared to other sensors in the literature (Table S4). The results above demonstrated that the Y-CD system can act as a unique turn-on fluorescent sensor for monitoring of His in biomedical analysis.

Scheme 2. Schematic Illustrating the Sensing Mechanism of Y-CDs to FQs and Y-CDs–FQs to His

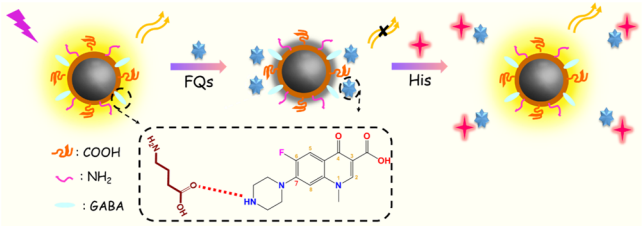

3.5. Detection of FQs in Real Sample Analysis. We further studied the practicality of the Y-CD fluorescence probe by detecting FQs in real sample analysis including antibiotic tablets and milk samples. The antibiotics NOR, CIP, and OFX were purchased from a local pharmacy and the milk was acquired from the supermarket. Table 2 summarized the results of fluorescence measurement before and after the standard addition method. They showed that the method was successful for the detection of antibiotics and free from interference of excipients. The satisfactory recoveries of NOR, CIP, and OFX in the proposed method were 95.8–102.4%, with RSDs of 3.6–5.4%. In addition, when separately spiking three FQs with three levels (0.5, 5, and 10 μM) in milk samples, the average recoveries were achieved, such as 96–101.2% for NOR, 92–98.8% for CIP, and 94–101.8% for OFX, and all RSDs were found lower than 6.6% (Table 2). Hence, the results suggest that the proposed method is practicable and reliable.

3.6. Imaging of His in Living Cell Systems. These results highlight that the Y-CDs are an excellent multifunctional sensing platform and can also be utilized as a new fluorescence tag for cell imaging applications. First, human hepatoma SMMC 7721 cells were chosen as a model in vivo system for appraising the potential of Y-CDs in cell imaging. We used the standard MTT assay to explore the cytotoxicity of Y-CDs. Figure S13 describes that the viability of SMMC 7721

DOI: 10.1021/acsami.8b16710
ACS Appl. Mater. Interfaces 2018, 10, 42915–42924

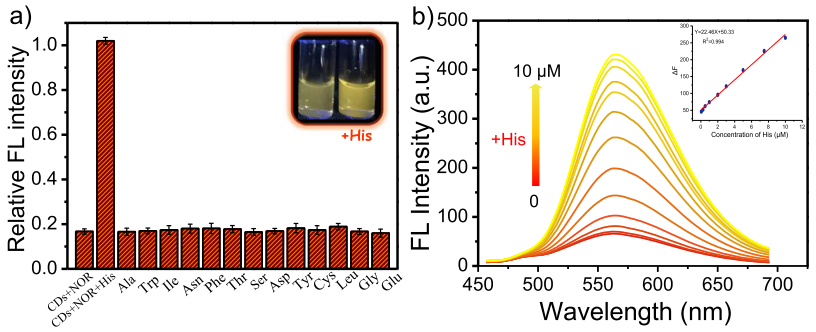

Figure 4. (a) Relative FL intensity of Y-CDs in the presence of different amino acids. Inserts are the photographs of Y-CD−NOR solution before and after adding His under 365 nm UV light. (b) FL recovery of Y-CDs−NOR (0.2 mg·mL^{-1} and 50 μM, respectively) in the presence of various concentrations of His. Insert: linear curve of FL restorations of Y-CDs−NOR.

Table 2. Recoveries Test of Three FQs in the Tablets and Milk Samples with the Standard Addition Method Based on the Y-CD Probe (n = 3)

analytes	spiked level (μmol L^{-1})	found (μmol L^{-1})	recovery (%)	RSD (%)
		Tablets		
NOR	5	4.79	95.8	3.6
CIP	5	5.12	102.4	4.6
OFX	5	4.87	97.4	5.4
		Milk Samples		
NOR	0.5	0.48	96	4.9
	5	5.08	101.6	5.6
	10	10.12	101.2	3.4
CIP	0.5	0.46	92	6.6
	5	4.85	97	4.5
	10	9.88	98.8	4.7
OFX	0.5	0.47	94	5.3
	5	5.04	101.8	6.1
	10	9.75	97.5	4.2

cell treatment with a wide concentration range of 50 to 1000 μg/mL of Y-CDs is more than 83% even exposure to a high concentration of 1000 μg/mL, which manifests the low toxicity of the Y-CDs and the promise of their exceptional potential for intracellular imaging of living cell systems. As shown in Figure 5a−c, the cells incubated with Y-CDs show yellow fluorescence. It can be concluded that Y-CDs demonstrate good cell permeability and efficiently accumulate in the cell membrane, cytoplasm and even inside the cell nucleus. Figure 5d shows obvious fluorescence quenching after adding 50 μM NOR in cells. With further incubation of the cells with His, the intracellular FL signal could be turned on gradually with an increase of the concentration of His (Figure 5e,f), proving that the process of fluorescence change in vivo was in accordance with that in vitro. These results imply that the Y-CDs−NOR sensing platform can be utilized to image the intracellular His level in living cells.

4. CONCLUSIONS

In brief, we synthesized Y-CDs with yellow emission by the one-pot hydrothermal method using *o*-PD and GABA as precursors. The obtained Y-CDs displayed an excellent multifunctional sensing capability for analysis of FQs and His. In the presence of FQs, the fluorescence of Y-CDs can be distinctly decreased by static quenching because of the specific interaction between piperazine on the C7 position of FQs and the active structures on the surface of Y-CDs. By adding His to

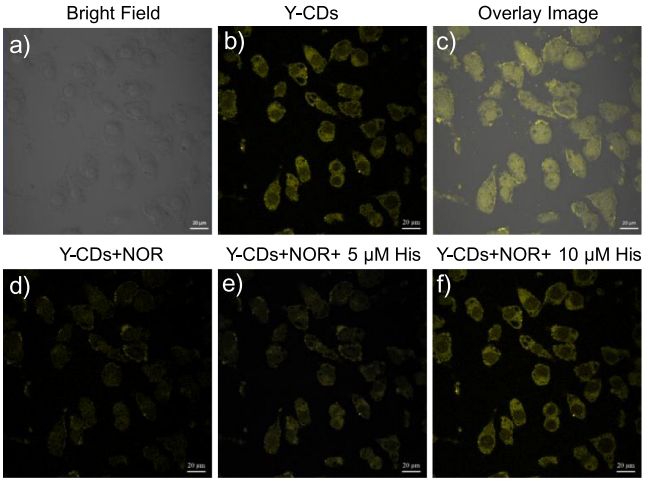

Figure 5. LSCM images of SMMC 7721 cells (a) bright field, (b) treated with 0.2 mg mL^{-1} Y-CDs, (c) overlay images of (a,b), (d) with 0.2 mg mL^{-1} Y-CDs and 50 μM NOR, and (e,f) with Y-CDs−NOR and His (5 and 10 μM).

the Y-CDs−FQs system, FQs will combine with His and form a more stable complex FQs−His, which recovers the surface states of Y-CDs and enhances the fluorescence. Therefore, based on the satisfactory selectivity and sensitivity, the method has been validated for screening FQs in real samples and live cell imaging for detection of His. Moreover, this sensing platform has a great potential for widespread use in clinical diagnostics and environmental analysis.

■ ASSOCIATED CONTENT

Supporting Information

The Supporting Information is available free of charge on the ACS Publications website at DOI: 10.1021/acsami.8b16710.

Experimental details; elemental analysis, XPS spectra of N 1s and O 1s of Y-CDs; fluorescence emission spectra of Y-CDs under the different excitation wavelengths; effect of time intervals of irradiation, pH, and ionic strength on FL intensity of Y-CDs; fluorescence lifetime; chemical structures of FQs; UV−vis absorption of the Y-CDs before and after adding NOR and His; FTIR spectra of GABA, Y-CDs, A-CDs, and R-CDs; effect of pH and potentially interfering substances on FL intensity of the Y-CD sensing system; and cytotoxicity testing results of Y-CDs and comparison of the detection

DOI: 10.1021/acsami.8b16710
ACS Appl. Mater. Interfaces 2018, 10, 42915−42924

limits of FQs and His from various analytical methods (PDF)

AUTHOR INFORMATION

Corresponding Authors

*E-mail: dc@sxu.edu.cn. Phone: +86-351-7018613. Fax: +86-351-7018613 (C.D.).

*E-mail: licz@fiu.edu. Phone: +1 305 348 0120: Fax: +1-3053486954 (C.-z.L.).

ORCID

Chuan Dong: 0000-0002-1827-8794

Chen-zhong Li: 0000-0002-0486-4530

Notes

The authors declare no competing financial interest.

‖Exchange student on visit to Florida International University.

ACKNOWLEDGMENTS

We would like to thank the Department of Chemistry and Biochemistry at FIU for their technical support. The authors would also like to acknowledge the technical help of Ya-Li Hsu (the engineer of the Department of Chemistry & Biochemistry) and the writing support of Laura Keepax. This work was supported by the National Natural Science Foundation of China (nos. 21475080, 21575084, and 21729501), Shanxi Province Hundred Talents Project, and the Engineering Research Center Program of the National Science Foundation under the NSF Cooperative Agreement (no. EEC-1648451 and no. EEC-1647837). Dr. Li also thanks the support sponsored by the NSF Independent Research/Development (IRD) Program.

REFERENCES

(1) Ceyssens, P.-J.; Van Bambeke, F.; Mattheus, W.; Bertrand, S.; Fux, F.; Van Bossuyt, E.; Damée, S.; Nyssen, H.-J.; De Craeye, S.; Verhaegen, J.; The Belgian Streptococcus pneumoniae Study; Tulkens, P. M.; Vanhoof, R. Molecular Analysis of Rising Fluoroquinolone Resistance in Belgian Non-Invasive Streptococcus pneumoniae Isolates (1995-2014). *PLoS One* **2016**, *11*, e0154816.

(2) Bearden, D. T.; Danziger, L. H. Mechanism of Action of and Resistance to Quinolones. *Pharmacotherapy* **2012**, *21*, 224S−232S.

(3) Takahashi, H.; Hayakawa, I.; Akimoto, T. The History of the Development and Changes of Quinolone Antibacterial Agents. *Yakushigaku Zasshi* **2003**, *38*, 161−179.

(4) Hoof, N. V.; Wasch, K. D.; Okerman, L.; Reybroeck, W.; Poelmans, S.; Noppe, H.; Brabander, H. D. Validation of a liquid chromatography-tandem mass spectrometric method for the quantification of eight quinolones in bovine muscle, milk and aquacultured products. *Anal. Chim. Acta* **2005**, *529*, 265−272.

(5) Jeong, S.-H.; Song, Y.-K.; Cho, J.-H. Risk Assessment of Ciprofloxacin, Flavomycin, Olaquindox and Colistin Sulfate based on Microbiological Impact on Human Gut Biota. *Regul. Toxicol. Pharmacol.* **2009**, *53*, 209−216.

(6) Passerini de Rossi, B.; García, C.; Calenda, M.; Vay, C.; Franco, M. Activity of Levofloxacin and Ciprofloxacin on Biofilms and Planktonic Cells of Stenotrophomonas Maltophilia Isolates from Patients with Device-associated Infections. *Int. J. Antimicrob. Agents* **2009**, *34*, 260−264.

(7) DeWitte, B.; Dewulf, J.; Demeestere, K.; Van De Vyvere, V.; De Wispelaere, P.; Van Langenhove, H. Ozonation of Ciprofloxacin in Water: HRMS Identification of Reaction Products and Pathways. *Environ. Sci. Technol.* **2008**, *42*, 4889−4895.

(8) Liu, W.; Zhang, J.; Zhang, C.; Ren, L. Sorption of Norfloxacin by Lotus Stalk-based Activated Carbon and Iron-doped Activated Alumina: Mechanisms, Isotherms and Kinetics. *Chem. Eng. J.* **2011**, *171*, 431−438.

(9) Lavaee, P.; Danesh, N. M.; Ramezani, M.; Abnous, K.; Taghdisi, S. M. Colorimetric Aptamer based Assay for the Determination of Fluoroquinolones by Triggering the Reduction-catalyzing Activity of Gold Nanoparticles. *Microchim. Acta* **2017**, *184*, 2039−2045.

(10) Suryoprabowo, S.; Liu, L.; Peng, J.; Kuang, H.; Xu, C. Development of a Broad Specific Monoclonal Antibody for Fluoroquinolone Analysis. *Food Anal. Methods* **2014**, *7*, 2163−2168.

(11) Liu, X.; Steele, J. C.; Meng, X.-Z. Usage, Residue, and Human Health Risk of Antibiotics in Chinese Aquaculture: A review. *Environ. Pollut.* **2017**, *223*, 161−169.

(12) Li, Q.; Gao, J.; Zhang, Q.; Liang, L.; Tao, H. Distribution and Risk Assessment of Antibiotics in a Typical River in North China Plain. *Bull. Environ. Contam. Toxicol.* **2017**, *98*, 478−483.

(13) Codex Alimentarius Commission. *Joint FAO/WHO Food Standards Programme*: Rome, Italy, 2012.

(14) The Ministry of Agriculture. *Gazette of the Ministry of Agriculture of The People's Republic of China*, No. 2292: Beijing, China, 2015.

(15) Evaggelopoulou, E. N.; Samanidou, V. F. HPLC Confirmatory Method Development for the Determination of Seven Quinolones in Salmon Tissue (Salmo salar L.) Validated According to the European Union Decision 2002/657/EC. *Food Chem.* **2013**, *136*, 479−484.

(16) Rocha, D. G.; Santos, F. A.; da Silva, J. C. C.; Augusti, R.; Faria, A. F. Multiresidue Determination of Fluoroquinolones in Poultry Muscle and Kidney According to the Regulation 2002/657/EC. A Systematic Comparison of Two Different Approaches: Liquid Chromatography Coupled to High-Resolution Mass Spectrometry or Tandem Mass Spectrometry. *J. Chromatogr. A* **2015**, *1379*, 83−91.

(17) Alcaráz, M. R.; Vera-Candioti, L.; Culzoni, M. J.; Goicoechea, H. C. Ultrafast quantitation of six quinolones in water samples by second-order capillary electrophoresis data modeling with multivariate curve resolution-alternating least squares. *Anal. Bioanal. Chem.* **2014**, *406*, 2571−2580.

(18) Li, Y.-T.; Qu, L.-L.; Li, D.-W.; Song, Q.-X.; Fathi, F.; Long, Y.-T. Rapid and sensitive in-situ detection of polar antibiotics in water using a disposable Ag-graphene sensor based on electrophoretic preconcentration and surface-enhanced Raman spectroscopy. *Biosens. Bioelectron.* **2013**, *43*, 94−100.

(19) Vega, D.; Agüí, L.; González-Cortés, A.; Yáñez-Sedeño, P.; Pingarrón, J. M. Voltammetry and Amperometric Detection of Tetracyclines at Multi-wall Carbon Nanotube Modified Electrodes. *Anal. Bioanal. Chem.* **2007**, *389*, 951−958.

(20) Aga, D. S.; Goldfish, R.; Kulshrestha, P. Application of ELISA in Determining the Fate of Tetracyclines in Land-applied Livestock Wastes. *Analyst* **2003**, *128*, 658−662.

(21) Peng, J.; Kong, D.; Liu, L.; Song, S.; Kuang, H.; Xu, C. Determination of Quinoxaline Antibiotics in Fish Feed by Enzyme-Linked Immunosorbent Assay Using a Monoclonal Antibody. *Anal. Methods* **2015**, *7*, 5204−5209.

(22) Tang, Y.; Liu, H.; Gao, J.; Liu, X.; Gao, X.; Lu, X.; Fang, G.; Wang, J.; Li, J. Upconversion Particle@Fe_3O_4@Molecularly Imprinted Polymer with Controllable Shell Thickness as High-Performance Fluorescent Probe for Sensing Quinolones. *Talanta* **2018**, *181*, 95−103.

(23) Mao, B.; Qu, F.; Zhu, S.; You, J. Fluorescence Turn-On Strategy based on Silver Nanoclusters-Cu^{2+} System for Trace Detection of Quinolones. *Sens. Actuators, B* **2016**, *234*, 338−344.

(24) Chen, Z.; Qian, S.; Chen, J.; Cai, J.; Wu, S.; Cai, Z. Protein-templated Gold Nanoclusters based Sensor for Off-On Detection of Ciprofloxacin with a High Selectivity. *Talanta* **2012**, *94*, 240−245.

(25) Attia, M. S.; Essawy, A. A.; Youssef, A. O. Europium-sensitized and Simultaneous pH-assisted Spectrofluorimetric Assessment of Ciprofloxacin, Norfloxacin and Gatifloxacin in Pharmaceutical and Serum Samples. *J. Photochem. Photobiol., A* **2012**, *236*, 26−34.

(26) Kusakari, Y.; Nishikawa, S.; Ishiguro, S.-i.; Tamai, M. Histidine-like Immunoreactivity in the Rat Retina. *Curr. Eye Res.* **1997**, *16*, 600−604.

DOI: 10.1021/acsami.8b16710
ACS Appl. Mater. Interfaces 2018, 10, 42915−42924

(27) Kopple, J. D.; Swendseid, M. E. Evidence that Histidine is an Essential Amino Acid in Normal and Chronically Uremic Man. *J. Clin. Invest.* **1975**, *55*, 881−891.
(28) Jones, A. L.; Hulett, M. D.; Parish, C. R. Histidine-rich Glycoprotein: A Novel Adaptor Protein in Plasma that Modulates the Immune, Vascular and Coagulation Systems. *Immunol. Cell Biol.* **2005**, *83*, 106−118.
(29) Seshadri, S.; Beiser, A.; Selhub, J.; Jacques, P. F.; Rosenberg, I. H.; D'Agostino, R. B.; Wilson, P. W. F.; Wolf, P. A. Plasma Homocysteine as a Risk Factor for Dementia and Alzheimer's Disease. *N. Engl. J. Med.* **2002**, *346*, 476−483.
(30) Verri, C.; Roz, L.; Conte, D.; Liloglou, T.; Livio, A.; Vesin, A.; Fabbri, A.; Andriani, F.; Brambilla, C.; Tavecchio, L.; Calarco, G.; Calabrò, E.; Mancini, A.; Tosi, D.; Bossi, P.; Field, J. K.; Brambilla, E.; Sozzi, G. Fragile Histidine Triad Gene Inactivation in Lung Cancer. *Am. J. Respir. Crit. Care Med.* **2009**, *179*, 396−401.
(31) Zhang, L.-Y.; Sun, M.-X. Determination of Histamine and Histidine by Capillary Zone Electrophoresis with Pre-column Naphthalene-2,3-dicarboxaldehyde Derivatization and Fluorescence Detection. *J. Chromatogr. A* **2004**, *1040*, 133−140.
(32) Tateda, N.; Matsuhisa, K.; Hasebe, K.; Kitajima, N.; Miura, T. High-Performance Liquid Chromatographic Method for Rapid and Highly Sensitive Determination of Histidine using Postcolumn Fluorescence Detection with o-Phthaldialdehyde. *J. Chromatogr. B: Biomed. Sci. Appl.* **1998**, *718*, 235−241.
(33) Bae, D. R.; Han, W. S.; Lim, J. M.; Kang, S.; Lee, J. Y.; Kang, D.; Jung, J. H. Lysine-Functionalized Silver Nanoparticles for Visual Detection and Separation of Histidine and Histidine-Tagged Proteins. *Langmuir* **2010**, *26*, 2181−2185.
(34) Shahlaei, M.; Gholivand, M. B.; Pourhossein, A. Simultaneous Determination of Tyrosine and Histidine by Differential Pulse Cathodic Stripping Voltammetry Using H-point Standard Addition Method in Tap and Seawater. *Electroanalysis* **2009**, *21*, 2499−2502.
(35) Zheng, X.; Yao, T.; Zhu, Y.; Shi, S. Cu^{2+} Modulated Silver Nanoclusters as an On-Off-On Fluorescence Probe for the Selective Detection of L-histidine. *Biosens. Bioelectron.* **2015**, *66*, 103−108.
(36) Wu, C.; Fan, D.; Zhou, C.; Liu, Y.; Wang, E. Colorimetric Strategy for Highly Sensitive and Selective Simultaneous Detection of Histidine and Cysteine Based on G-Quadruplex-Cu(II) Metalloenzyme. *Anal. Chem.* **2016**, *88*, 2899−2903.
(37) Un, H.-I.; Wu, S.; Huang, C.-B.; Xu, Z.; Xu, L. A naphthalimide-based fluorescent probe for highly selective detection of histidine in aqueous solution and its application in in vivo imaging. *Chem. Commun.* **2015**, *51*, 3143−3146.
(38) Bian, W.; Wang, F.; Wei, Y.; Wang, L.; Liu, Q.; Dong, W.; Shuang, S.; Choi, M. M. F. Doped Zinc Sulfide Quantum Dots Based Phosphorescence Turn-Off/On Probe for Detecting Histidine in Biological Fluid. *Anal. Chim. Acta* **2015**, *856*, 82−89.
(39) Zhu, X.; Zhao, T.; Nie, Z.; Miao, Z.; Liu, Y.; Yao, S. Nitrogen-Doped Carbon Nanoparticle Modulated Turn-On Fluorescent Probes for Histidine Detection and Its Imaging in Living Cells. *Nanoscale* **2016**, *8*, 2205−2211.
(40) Zheng, X. T.; Ananthanarayanan, A.; Luo, K. Q.; Chen, P. Glowing Graphene Quantum Dots and Carbon Dots: Properties, Syntheses, and Biological Applications. *Small* **2014**, *11*, 1620−1636.
(41) Zhu, X.; Hondroulis, E.; Liu, W.; Li, C.-z. Biosensing Approaches for Rapid Genotoxicity and Cytotoxicity Assays upon Nanomaterial Exposure. *Small* **2013**, *9*, 1821−1830.
(42) Shah, P.; Zhu, X.; Zhang, X.; He, J.; Li, C.-z. Micro-electromechanical System-Based Sensing Arrays for Comparative in Vitro Nanotoxicity Assessment at Single Cell and Small Cell-Population Using Electrochemical Impedance Spectroscopy. *ACS Appl. Mater. Interfaces* **2016**, *8*, 5804−5812.
(43) Feng, H.; Qian, Z. Functional Carbon Quantum Dots: A Versatile Platform for Chemosensing and Biosensing. *Chem. Rec.* **2018**, *18*, 491−505.
(44) Chen, G.; Feng, H.; Jiang, X.; Xu, J.; Pan, S.; Qian, Z. Redox-Controlled Fluorescent Nanoswitch Based on Reversible Disulfide and Its Application in Butyrylcholinesterase Activity Assay. *Anal. Chem.* **2018**, *90*, 1643−1651.
(45) Sun, Q.; Fang, S.; Fang, Y.; Qian, Z.; Feng, H. Fluorometric detection of cholesterol based on β-cyclodextrin functionalized carbon quantum dots via competitive host-guest recognition. *Talanta* **2017**, *167*, 513−519.
(46) Ao, H.; Feng, H.; Huang, X.; Zhao, M.; Qian, Z. A reversible fluorescence nanoswitch based on dynamic covalent B-O bonds using functional carbon quantum dots and its application for α-glucosidase activity monitoring. *J. Mater. Chem. C* **2017**, *5*, 2826−2832.
(47) Tang, C.; Zhou, J.; Qian, Z.; Ma, Y.; Huang, Y.; Feng, H. A universal fluorometric assay strategy for glycosidases based on functional carbon quantum dots: β-galactosidase activity detection in vitro and in living cells. *J. Mater. Chem. B* **2017**, *5*, 1971−1979.
(48) Peng, Z.; Han, X.; Li, S.; Al-Youbi, A. O.; Bashammakh, A. S.; El-Shahawi, M. S.; Leblanc, R. M. Carbon dots: Biomacromolecule Interaction, Bioimaging and Nanomedicine. *Coord. Chem. Rev.* **2017**, *343*, 256−277.
(49) Nie, H.; Li, M.; Li, Q.; Liang, S.; Tan, Y.; Sheng, L.; Shi, W.; Zhang, S. X.-A. Carbon Dots with Continuously Tunable Full-Color Emission and Their Application in Ratiometric pH Sensing. *Chem. Mater.* **2014**, *26*, 3104−3112.
(50) Dong, Y.; Pang, H.; Yang, H. B.; Guo, C.; Shao, J.; Chi, Y.; Li, C. M.; Yu, T. Carbon-Based Dots Co-doped with Nitrogen and Sulfur for High Quantum Yield and Excitation-Independent Emission. *Angew. Chem., Int. Ed.* **2013**, *52*, 7800−7804.
(51) Yuan, Y. H.; Liu, Z. X.; Li, R. S.; Zou, H. Y.; Lin, M.; Liu, H.; Huang, C. Z. Synthesis of Nitrogen-doping Carbon Dots with Different Photoluminescence Properties by Controlling the Surface States. *Nanoscale* **2016**, *8*, 6770−6776.
(52) Carrara, S.; Arcudi, F.; Prato, M.; De Cola, L. Amine-Rich Nitrogen-Doped Carbon Nanodots as a Platform for Self-Enhancing Electrochemiluminescence. *Angew. Chem., Int. Ed.* **2017**, *56*, 4757−4761.
(53) Feng, T.; Ai, X.; An, G.; Yang, P.; Zhao, Y. Charge-Convertible Carbon Dots for Imaging-Guided Drug Delivery with Enhanced in Vivo Cancer Therapeutic Efficiency. *ACS Nano* **2016**, *10*, 4410−4420.
(54) Hou, P.; Yang, T.; Liu, H.; Li, Y. F.; Huang, C. Z. An Active Structure Preservation Method for Developing Functional Graphitic Carbon Dots as an Effective Antibacterial Agent and a Sensitive pH and Al(iii) Nanosensor. *Nanoscale* **2017**, *9*, 17334−17341.
(55) Cheng, L.; Li, Y.; Zhai, X.; Xu, B.; Cao, Z.; Liu, W. Polycation-b-Polyzwitterion Copolymer Grafted Luminescent Carbon Dots As a Multifunctional Platform for Serum-Resistant Gene Delivery and Bioimaging. *ACS Appl. Mater. Interfaces* **2014**, *6*, 20487−20497.
(56) Gao, X. M.; Yang, L.; Zheng, Y.; Yang, X. X.; Zou, H. Y.; Han, J.; Liu, Z. X.; Li, Y. F.; Huang, C. Z. "Click" on Alkynylated Carbon Quantum Dots: An Efficient Surface Functionalization for Specific Biosensing and Bioimaging. *Chem.—Eur. J.* **2016**, *23*, 2171−2178.
(57) Gao, D.; Zhao, H.; Chen, X.; Fan, H. Recent Advance in Red-Emissive Carbon Dots and Their Photoluminescent Mechanisms. *Mater. Today Chem.* **2018**, *9*, 103−113.
(58) Qu, F.; Sun, Z.; Liu, D.; Zhao, X.; You, J. Direct and Indirect Fluorescent Detection of Tetracyclines Using Dually Emitting Carbon Dots. *Microchim. Acta* **2016**, *183*, 2547−2553.
(59) Ding, H.; Yu, S.-B.; Wei, J.-S.; Xiong, H.-M. Full-Color Light-Emitting Carbon Dots with a Surface-State-Controlled Luminescence Mechanism. *ACS Nano* **2016**, *10*, 484−491.
(60) Gao, W.; Song, H.; Wang, X.; Liu, X.; Pang, X.; Zhou, Y.; Gao, B.; Peng, X. Carbon Dots with Red Emission for Sensing of Pt^{2+}, Au^{3+}, and Pd^{2+} and Their Bioapplications in Vitro and in Vivo. *ACS Appl. Mater. Interfaces* **2018**, *10*, 1147−1154.
(61) Jiang, K.; Sun, S.; Zhang, L.; Wang, Y.; Cai, C.; Lin, H. Bright-Yellow-Emissive N-Doped Carbon Dots: Preparation, Cellular Imaging, and Bifunctional Sensing. *ACS Appl. Mater. Interfaces* **2015**, *7*, 23231−23238.
(62) Lu, W.; Li, Y.; Li, R.; Shuang, S.; Dong, C.; Cai, Z. Facile Synthesis of N-Doped Carbon Dots as a New Matrix for Detection of

DOI: 10.1021/acsami.8b16710
ACS Appl. Mater. Interfaces 2018, 10, 42915−42924

Hydroxy-Polycyclic Aromatic Hydrocarbons by Negative-Ion Matrix-Assisted Laser Desorption/Ionization Time-of-Flight Mass Spectrometry. *ACS Appl. Mater. Interfaces* **2016**, *8*, 12976−12984.
(63) Lu, W.; Gao, Y.; Jiao, Y.; Shuang, S.; Li, C.; Dong, C. Carbon Nano-dots as a Fluorescent and Colorimetric Dual-readout Probe for the Detection of Arginine and Cu^{2+} and Its Logic Gate Operation. *Nanoscale* **2017**, *9*, 11545−11552.
(64) Shi, B.; Su, Y.; Zhang, L.; Huang, M.; Liu, R.; Zhao, S. Nitrogen and Phosphorus Co-Doped Carbon Nanodots as a Novel Fluorescent Probe for Highly Sensitive Detection of Fe^{3+} in Human Serum and Living Cells. *ACS Appl. Mater. Interfaces* **2016**, *8*, 10717−10725.
(65) Chen, Y.; Lian, H.; Wei, Y.; He, X.; Chen, Y.; Wang, B.; Zeng, Q.; Lin, J. Concentration-Induced Multi-Colored Emissions in Carbon Dots: Origination from Triple Fluorescent Centers. *Nanoscale* **2018**, *10*, 6734−6743.
(66) Yuan, K.; Zhang, X.; Qin, R.; Ji, X.; Cheng, Y.; Li, L.; Yang, X.; Lu, Z.; Liu, H. Surface States Modulation of Red Emitting Carbon Dots for White Light-Emitting Diode. *J. Mater. Chem. C* **2018**, DOI: 10.1039/C8TC04468F.
(67) Schmuck, G.; Schürmann, A.; Schlüter, G. Determination of the Excitatory Potencies of Fluoroquinolones in the Central Nervous System by an In Vitro Model. *Antimicrob. Agents Chemother.* **1998**, *42*, 1831−1836.
(68) Sarro, A.; Sarro, G. Adverse Reactions to Fluoroquinolones. An Overview on Mechanistic Aspects. *Curr. Med. Chem.* **2001**, *8*, 371−384.
(69) Zhang, Q.; Fang, H.; Zhang, H.; Qin, D.; Hong, Z.; Du, Y. Vibrational Spectroscopic Characterization of the Co-Crystal and the Forming Condition between γ-Aminobutyric Acid and Benzoic Acid. *Spectrosc. Spectr. Anal.* **2017**, *37*, 3786−3792.
(70) Yan, C.; Liao, K.; Hu, Y.; Xu, Y. Histidine Photooxidation in Assessment of Photosensitizing Agents **1998**, *31*, 366-367.

DOI: 10.1021/acsami.8b16710
ACS Appl. Mater. Interfaces 2018, 10, 42915−42924